Electronic structure and transport properties of hydrogenated graphene and graphene nanoribbons

2010 New J. Phys. 12 125005

(http://iopscience.iop.org/1367-2630/12/12/125005)

New Journal of Physics
The open-access journal for physics

Electronic structure and transport properties of hydrogenated graphene and graphene nanoribbons

D H Choe, Junhyeok Bang and K J Chang[1]
Department of Physics, Korea Advanced Institute of Science and Technology, Daejeon 305-701, Korea
E-mail: kchang@kaist.ac.kr

New Journal of Physics **12** (2010) 125005 (16pp)
Received 25 June 2010
Published 13 December 2010
Online at http://www.njp.org/
doi:10.1088/1367-2630/12/12/125005

Abstract. The band gap opening is one of the important issues in applications of graphene and graphene nanoribbons (GNRs) to nanoscale electronic devices. As hydrogen strongly interacts with graphene and creates short-range disorder, the electronic structure is significantly modified by hydrogenation. Based on first-principles and tight-binding calculations, we investigate the electronic and transport properties of hydrogenated graphene and GNRs. In disordered graphene with low doses of H adsorbates, the low-energy states near the neutrality point are localized, and the degree of localization extends to high-energy states with increasing adsorbate density. To characterize the localization of eigenstates, we examine the inverse participation ratio and find that the localization is greatly enhanced for the defect levels, which are accumulated around the neutrality point. Our calculations support the previous result that even with a low dose of H adsorbates, graphene undergoes a metal–insulator transition. In GNRs, relaxations of the edge C atoms play a role in determining the edge structure and the hydrocarbon conformation at low and high H concentrations, respectively. In disordered nanoribbons, we find that the energy states near the neutrality point are localized and conductances through low-energy channels decay exponentially with sample size, similar to disordered graphene. For a given channel energy, the localization length tends to decrease as the adsorbate density increases. Moreover, the energy range of localization exceeds the intrinsic band gap.

[1] Author to whom any correspondence should be addressed.

Contents

1. Introduction

Graphene, a single layer of carbon atoms packed in a honeycomb lattice, has attracted much attention due to its remarkable electronic structure with a zero gap and quasiparticles described by massless Dirac fermions [1]. The low-energy electronic structure of graphene near the Brillouin zone corners is characterized by the linear dispersion, which leads to unusual transport properties such as an unconventional half-integer quantum Hall effect and perfect transmission through a potential barrier at normal incidence [2]–[4]. As compared to Si-based microelectronics, graphene has extremely high carrier mobility and thus high potential for applications to electronic devices [5]. However, due to the zero gap, pristine graphene cannot be used directly for conventional transistors. For practical applications, it is important to control the energy gap, carrier type and concentration of graphene systems.

Graphene nanoribbons (GNRs), as quasi-one-dimensional structures, were shown to have energy gaps, which arise from the quantum confinement effect and sensitively vary with the ribbon width [6]. In recent experiments [7, 8], GNRs with atomically smooth edges and narrow widths below 10 nm have been synthesized and high-performance transistor operations have been demonstrated. Other strategies were proposed to achieve the gap opening, based on the formation of periodic structures such as antidot lattices [9]–[11] or regular patterns of hydrogen-adsorbed regions [12]. The electronic structure of graphene can be modified by dosing with atoms or molecules. In particular, the chemical reaction of graphene with H, F, OH and CH_3 was shown to be significant because adsorbates interact directly with the C p_z orbitals perpendicular to the plane [13]. It was predicted that if graphene is fully hydrogenated, the metallic state turns into a band insulating phase with an energy gap of about 3.6 eV [14]. A metal–insulator transition, which was reversible in cycles of hydrogenation and annealing, was indeed observed in hydrogenated graphene with high coverages of H adsorbates [15]. Interestingly, a similar metal–insulator transition was reported in graphene with substantially low doses of hydrogen [16]. Recent theoretical calculations showed that the metal–insulator transition can occur by the localization of electron states in disordered graphene even with low H concentrations [17]. Using density functional calculations, there have been a series of theoretical studies of the structural properties of hydrogen adsorbed graphene [18, 19] and GNRs with the edges passivated hydrogen [20, 21] and the electronic properties of hydrogenated GNRs [22, 23].

In this work, we present the results of theoretical calculations for the electronic and transport properties of hydrogenated graphene and GNRs. Based on density functional and

tight-binding (TB) calculations, we discuss the energetics of different H adsorption sites, the gap opening and the formation of localized states near the neutrality point in graphene with low doses of H atoms. In armchair-shaped GNRs, we examine the bonding characteristics of various edge conformations by hydrogenation, the energetics of hydrocarbons and the localization behavior of low-energy states in disordered systems.

2. Calculation method

Our calculations are performed using a combined approach of the density-functional theory and the TB method. The electronic structures and total energies of hydrogenated graphene and GNRs are calculated using the generalized gradient approximation (GGA) [24] for the exchange-correlation potential and ultrasoft pseudopotentials [25] for the ionic potentials, as implemented in VASP code [26]. The wave functions are expanded in plane waves with a kinetic energy cutoff of 400 eV. For graphene, we use two 7×7 and 10×10 hexagonal supercells with a vacuum region of 10 Å, which ensures prohibiting interactions between adjacent planes, while an additional vacuum of 10 Å between neighboring edges is included in the supercell geometry of GNRs. The Brillouin zone integration is done using k-points generated by the $6 \times 6 \times 1$ and $3 \times 3 \times 1$ Monkhorst–Pack meshes [27] for the graphene 7×7 and 10×10 supercells, respectively, and by the $1 \times 9 \times 1$ mesh for the supercell with two unit cells of GNRs. All of the atomic positions are fully optimized until the residual forces are less than 0.02 eV Å^{-1}, and the lattice parameter along the axial direction is fixed as that (2.46 Å) of graphene. The energetics of various conformations in hydrogenated graphene and GNRs are examined by calculating the formation energies defined as

$$E_{\mathrm{f}} = E_{\mathrm{tot}}(\mathrm{C, H}) - N_{\mathrm{C}}\mu_{\mathrm{C}} - N_{\mathrm{H}}\mu_{\mathrm{H}}, \tag{1}$$

where $E_{\mathrm{tot}}(\mathrm{C, H})$ is the total energy of a supercell containing H adsorbates, N_i ($i = \mathrm{C}$ and H) is the number of species i in the supercell, and μ_i is the corresponding chemical potential. Here, we use the energies per atom of pristine graphene and an H_2 molecule for μ_{C} and μ_{H}, respectively.

The transport properties of disordered graphene and GNRs by hydrogenation are studied by calculating conductances based on the TB model. As hydrogen interacts with the C p_z orbitals, conductances are mostly affected for the π-orbital energies near the neutrality point. We consider a single-band TB Hamiltonian to describe interactions of graphene and GNRs with hydrogen,

$$\mathcal{H} = -\sum_{\langle l,m \rangle} \gamma_{l,m} C_l^{\dagger} C_m + \sum_n \mathcal{H}_n, \tag{2}$$

$$\mathcal{H}_n = \epsilon_{\mathrm{H}} d_n^{\dagger} d_n - \gamma_{\mathrm{H}} (C_{p_n}^{\dagger} d_n + C_{p_n} d_n^{\dagger}), \tag{3}$$

where $\gamma_{l,m}$ is the hopping integral between the nearest-neighbor C p_z orbitals, γ_{H} is the coupling strength between the C and H orbitals, and ϵ_{H} is the H on-site energy.

Here, C_l ($C_l^{\dagger}$) is the annihilation (creation) operator on the host lth site, d_n ($d_n^{\dagger}$) is the annihilation (creation) operator on the H site, and p_n is the host site bonded to the H atom. In graphene, we use the parameters of $\gamma_{l,m} = 2.6$ eV, $\gamma_{\mathrm{H}} = 5.72$ eV and $\epsilon_{\mathrm{H}} = 0$ eV, which are determined by fitting to the GGA band structure. In GNRs with each edge C atom passivated by a single H atom, the edge C atoms undergo large relaxations and thus have shorter C–C bond

lengths [6]. Using the hopping integral of $\gamma_{l,m} = 3.20\,\text{eV}$ between the edge C atoms, we obtain the variation of the band gap with the width, which is in good agreement with the GGA results.

For a device model, in which a disordered sample is sandwiched between two semi-infinite graphene or nanoribbon electrodes, the two-terminal conductance is calculated by using the Landauer–Büttiker formula, $g_{\text{L}} = 2\,\text{Tr}(tt^{\dagger})$, where t is the transmission matrix and the factor 2 accounts for spin degeneracy [28]. In graphene, periodic boundary conditions are imposed in the transverse direction to remove the effect of edge states, while they are not required in GNRs with the edge C atoms passivated by hydrogen. For the energetics of hydrogenated graphene and GNRs, in which the GGA calculations are used, we consider hydrogen adsorptions on both sides of the plane. On the other hand, to calculate conductances in disordered graphene and GNRs with small amounts of H adsorbates, we only consider hydrogen adsorption on one side of the plane because the TB approach cannot distinguish the difference between both sides. The details of the calculations are given elsewhere [17].

3. Results and discussion

3.1. Hydrogenated graphene

The bonding characteristics between graphene and adatoms depend on the type of adatoms. Metal adatoms belonging to groups I–III form ionic bonds with graphene at hexagon centers, while covalent bonds are preferable for transition, nobel and group-IV metals [29]. Hydrogen directly interacts with the p_z orbital of the C site, forming a strong C–H bond with a binding energy of about 0.8 eV. As the H-bonded C atom relaxes by 0.45 Å toward the H atom, the C–C–C bond angle decreases from 120° to 114.5°, and the H–C–C bond angle is about 103.7°. Thus, the bonding configuration changes from sp^2 to sp^3, in good agreement with previous studies [13, 15, 30, 31].

When a single H atom is adsorbed, the band gap is developed as the sublattice symmetry is broken, and a localized defect level appears at the neutrality point, as shown in figure 1(a). Note that the electronic structure resembles that of an isolated C-vacancy because the formation of the C–H bond effectively removes one C atom from the lattice. According to first-principles calculations [32], an isolated C-vacancy exhibits two localized states associated with the dangling bond σ- and π-orbitals around the vacancy site. The σ-orbital localized state is located right at the valence band edge, whereas the π-orbital localized state lies at 0.5 eV below the valence band maximum (VBM). However, in the TB model, the localized states are not correctly described because the σ-orbitals are ignored. Moreover, the π-orbital localized state is positioned at the neutrality point unless the TB model includes the second nearest-neighbor hopping parameter, which can shift the π-orbital localized state to lower energies [33]. In contrast to C-vacancy, a single H adsorbate has only the defect level at the neutrality point, which is associated with interactions between the H and C orbitals, without forming the σ-orbital localized state. Nevertheless, the characteristics of the localized state are similar to that of an ideal C-vacancy. The wave function amplitudes are zero in the same sublattice as the C site where H is adsorbed, whereas those in the opposite sublattice decay rapidly with distance from the adsorbate site [33, 34]. We check the charge distribution of the defect levels and the energy splitting at the neutrality point by H adsorbates, and find that the results of the TB model with only the first-neighbor coupling parameter $\gamma_{l,m}$ are in good agreement with the GGA calculations up to four H atoms (for example, see figure 1).

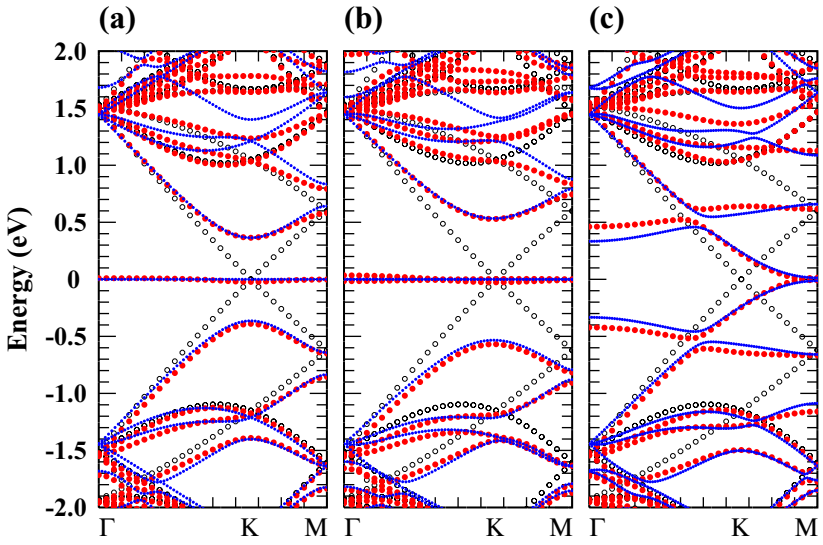

Figure 1. The band structures of graphene with (a) one H atom, (b) two H atoms in the same A sublattice and (c) two H atoms in both the A and B sublattices in the 7×7 supercell. Red and blue points represent the GGA and TB results for hydrogenated graphene, respectively, whereas black circles represent the GGA band structure of pristine graphene.

The effects of additional H atoms on the formation of the localized states and the gap opening strongly depend on their relative adsorption sites. Due to the unique wave function amplitudes, the localized states are decoupled if the H atoms are selectively adsorbed at the same sublattice sites, resulting in the nearly degenerate levels at the neutrality point (figure 1(b)). Meanwhile, the gap opening occurs with a tendency for increasing with n_{H}, where n_{H} is the ratio of the number of H adsorbates to the total number of C atoms. The energy gaps are estimated to be about 0.4, 0.5, 1.2 and 1.6 eV for $n_{\mathrm{H}} = 0.5$, 1, 5 and 10%, respectively. In the gap region, the densities of states are zero, while they exhibit sharp peaks superimposed at the neutrality point. On the other hand, if the H atoms are randomly adsorbed in both the A and B sublattices, interactions between the localized states are greatly enhanced, because of nonzero wave function amplitudes in the opposite sublattices. In contrast to adsorbates in the same sublattice, the gap opening does not take place (figure 1(c)). As the localized levels split, the finite densities of states appear for low energies near the neutrality point, similar to random C-vacancy defects [34]. It was shown that the energy range of the level splitting grows with increasing n_{H} [17].

We examine the energetics of two configurations for H adsorption, in which the H atoms are placed in the same sublattice or in both the A and B sublattices. In graphene with two H adsorbates, we choose a large 10×10 supercell to reduce interactions between the H atoms in neighboring supercells. The formation energies of a second H atom at various adsorption sites are compared in figure 2 with a first H atom fixed at an A sublattice site. In the former configuration, the formation energies are higher than that of two isolated H adsorbates. However, the energy differences are within 0.2 eV, nearly independent of the distance between the H atoms, in good agreement with the result that the localized states are decoupled. In the latter configuration, the formation energies are generally lowered mainly due to the level repulsion,

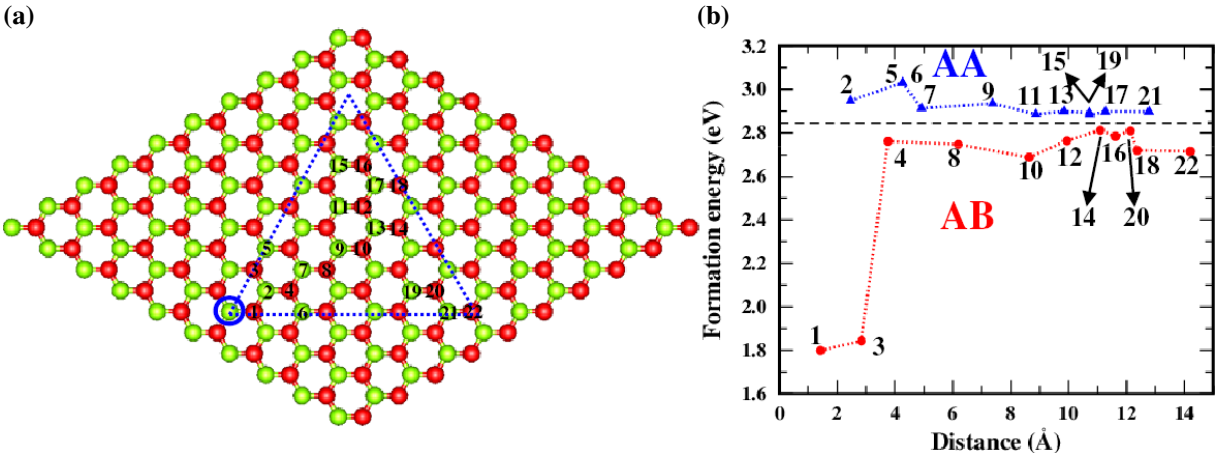

Figure 2. (a) Numbers denote various positions of a second H atom around a first H atom (blue circle at the *A* sublattice site) in the 10 × 10 supercell and (b) their formation energies per molecule are plotted as a function of the distance between the two H atoms. In (a), green and red balls denote the *A* and *B* sublattice sites, respectively. In (b), the dashed line represents the formation energy of two isolated H adsorbates, and *AA* and *AB* denote the sublattice sites of two H atoms.

compared with the former case, indicating that the selective dilution of H adsorbates is energetically unfavorable. Note that the formation energies relative to two isolated H adsorbates are lower by about 1.0 eV within the distance 3 Å. Thus, the second H atom prefers to reside at sites 1 and 3 in the vicinity of the first H atom. The two distinct hydrogen dimer structures at sites 1 and 3 are consistent with the ortho- and para-dimers, respectively, which were observed on the graphite (0001) surface adsorbed by hydrogen [35, 36]. As the H concentration increases, the formation of hydrogen dimers (figure 2(b)) is likely to occur. Actually, at very high H coverages, graphene was proposed to turn into a band insulator, known as graphane with band gaps of 3.5–3.7 eV [14]. On the other hand, at low doses of H adsorbates, it was suggested that a single absorbed H atom is more likely to desorb rather than to diffuse to form dimer structures with other H atoms, because the energy barrier is 1.14 eV for hydrogen diffusion, whereas the desorption barrier is 0.9 eV [36]. Interestingly, an insulating state was observed in hydrogenated graphene with substantially low doses, indicating that disorder induces a metal–insulator transition [16].

As the chemical reaction of hydrogen with graphene gives rise to short-range disorder potential, Dirac fermions can be localized due to the intervalley scattering between the two valleys, while the backscattering is suppressed in the presence of long-range disorders. Our previous calculations [17] showed that disordered graphene by hydrogenation undergoes a metal–insulator transition and that conductances in a narrow range of energies near the neutrality point decay exponentially with the sample size and are well fitted by one-parameter scaling function [37, 38]. To see more precisely the localization behavior of low-energy states, we investigate the characteristics of the wave functions in disordered graphene with low coverages of H adsorbates. The degree of localization for the eigenstates can be described by the

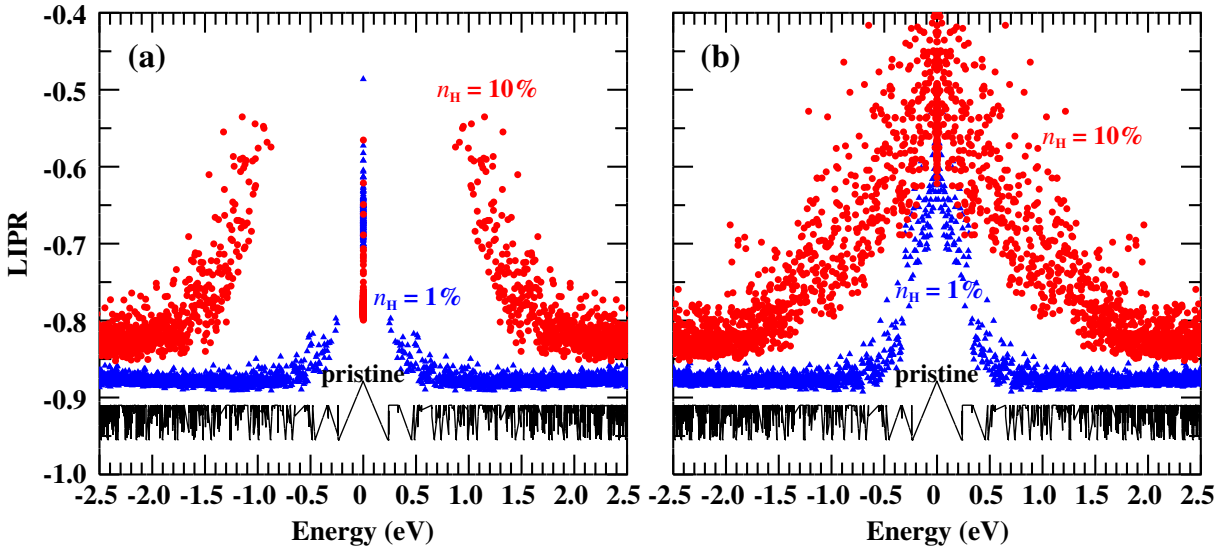

Figure 3. The LIPR is plotted as a function of energy for two disordered graphene systems, in which (a) the H atoms are random in one sublattice and (b) they are in both the A and B sublattices, with $n_H = 1\%$ (blue triangles) and 10% (red circles). Black lines represent the LIPR of pristine graphene.

normalized logarithm of the inverse participation ratio (LIPR) [39],

$$\mathrm{LIPR}(E) = \frac{\ln \mathcal{P}(E)}{\ln N}, \tag{4}$$

where the inverse participation ratio is defined as $\mathcal{P}(E) = \sum_{i=1}^{N} |\Psi_E(\mathbf{r}_i)|^4$, N is the number of basis orbitals in the TB Hamiltonian, which equals the number of sites, and $\Psi_E(\mathbf{r}_i)$ is the wave function amplitude at the ith site. The LIPR is close to -1 for an extended state as $\mathcal{P}(E) \sim N^{-1}$, while it increases to a higher value for a localized state because of the contribution from a finite number of lattice sites.

For graphene systems with a size of 14 nm, the LIPRs obtained by direct diagonalization in the TB model are plotted as a function of energy for $n_H = 1$ and 10% in figure 3. For two different configurations, where the H atoms are random only in one sublattice or in both the A and B sublattices, the LIPR values are found to be very high for energies near the neutrality point, implying that the states are localized by disorder, while they become significantly low for the extended states far from the neutrality point. It is clear that the energy gaps, where the LIPR is not defined, are developed in the former configuration, consistent with the result that the density of states is zero in the gap region, with only sharp peaks at the neutrality point. In addition, the energy states around the band edges become localized, and the degree of localization increases with increasing n_H. Indeed, conductances through the band edge states were shown to be significantly suppressed as n_H increases [17]. In the latter configuration, the LIPR also exhibits increasing behavior for energy states around the neutrality point due to the localized states. Without the gap opening, the LIPR increases very rapidly as the energy becomes close to the neutrality point. Thus, the disorder effect on conductance is more significant for low-energy states. As n_H increases from 1 to 10%, the localization is extended to high-energy states. In the previous study, we examined the variation of conductance with sample

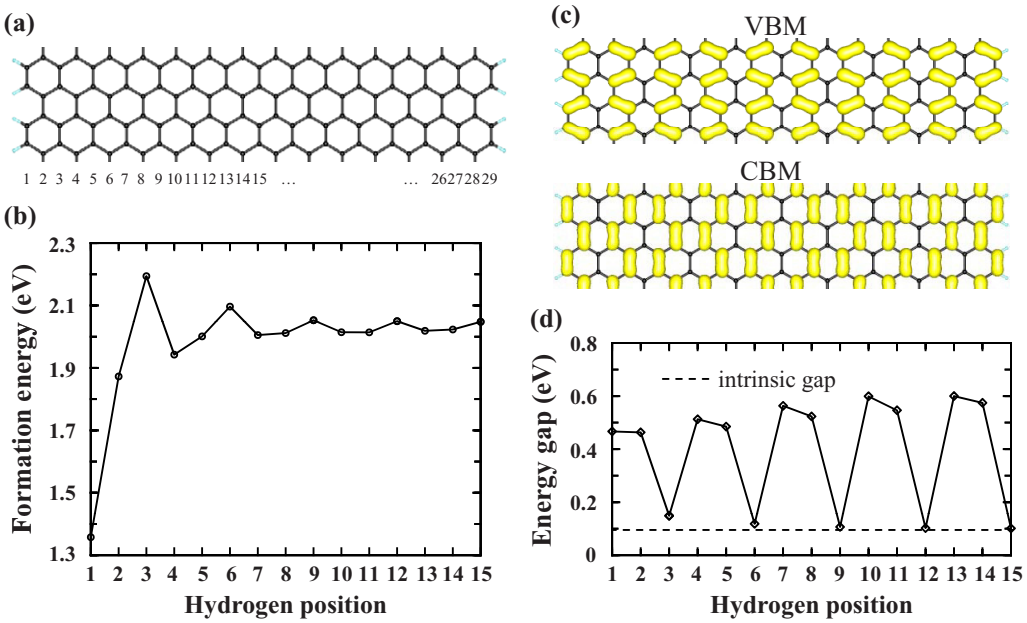

Figure 4. (a) The supercell structure with two unit cells of pristine 29-AGNR, with the dimer lines indexed by numbers, and (b) the formation energies per atom at different line positions of a single H adsorbate in (a). (c) The charge densities of the VBM and CBM states in pristine 29-AGNR and (d) the variation in the energy gap with the H adsorption position in (a). In (a) and (c), blue dots represent the H atoms, which passivate the edge dangling bonds.

size in disordered graphene with $n_H = 10\%$, and found that the localization lengths are 2–7 nm in the energy range of 0.8 eV, exhibiting increasing behavior with the channel energy [17]. This behavior is consistent with the results for the LIPR.

3.2. Hydrogenated graphene nanoribbons (GNRs)

GNRs have two types of fundamental edge shape, zigzag and armchair, and the electronic structures depend on their widths and orientations. Here, we consider the adsorption of H atoms on armchair-shaped GNRs, which have larger band gaps than zigzag-shaped GNRs. We define pristine armchair graphene nanoribbons (n-AGNRs) as those that have all the edge dangling bonds passivated with a single H atom per edge C atom, where n denotes the number of C–C dimer lines. Figure 4(a) shows the supercell of 29-AGNR with two unit cells. In 29-AGNR with one H adsorbate, the formation energies defined in equation (1) are compared for different adsorption sites in figure 4(b). At the edge sites, hydrogen breaks two carbon π-bonds to form the sp^3 hybridization, while three carbon π-bonds are broken at the inner sites of n-AGNR [23]. The H–C–C bond angles are estimated to be 109.8° and 103.0–104.6° at the edge and inner sites, respectively. Moreover, the edge site accommodates the structural relaxations more easily due to the nearby vacuum region. Thus, hydrogen prefers to reside on top of the edge C atoms rather than at the inner host atoms. Note that the peaks appear at the $3n$ positions in the formation energy curve. These peaks are related to the charge densities of the VBM and conduction band minimum (CBM) states (figure 4(c)), which exhibit the density nodes in the $3n$ lines. If hydrogen

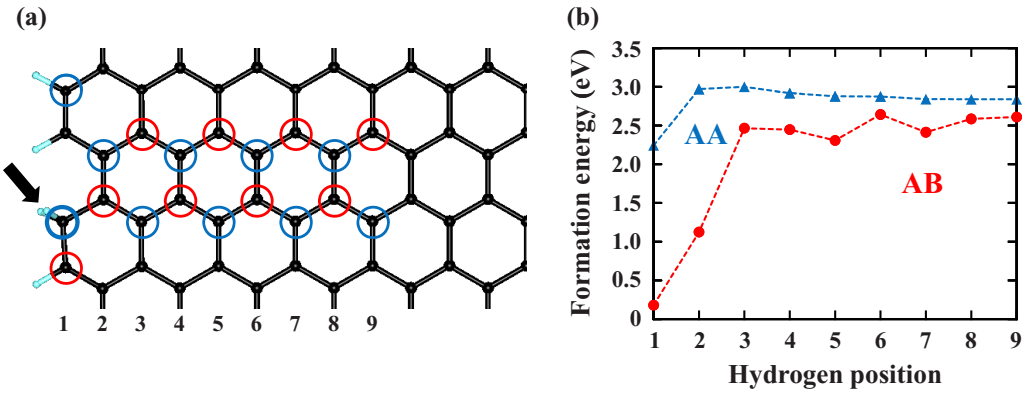

Figure 5. (a) Possible positions of a second H adsorbate in the supercell with two unit cells of 29-AGNR, in which a first H adsorbate is located at the edge site (indicated by arrow) in the *A* sublattice. Blue and red circles denote the *A* and *B* sublattice sites, respectively. (b) The formation energies per molecule are plotted for different positions of two H adsorbates in the C–C dimer lines indexed by numbers in (a).

is adsorbed at the charge density nodes, interactions between hydrogen and *n*-AGNR are greatly reduced, resulting in a weaker C–H bond and thereby a higher formation energy. This feature is also reflected by the oscillatory variation of the energy gap with the H position in figure 4(d). At the $3n$ positions, the gap size is almost equal to the value of 0.1 eV for pristine 29-AGNR, while it is enhanced to 0.5–0.6 eV for other adsorption sites.

When a second H atom is adsorbed, the formation energy depends on the configuration of two H adsorbates. Figure 5 shows the formation energies of a second H atom at different positions, with a first H atom bound to the edge C atom in the *A* sublattice. The formation energies are generally lower when two adsorbates are positioned at the *A* and *B* sublattice sites, because of the stronger coupling between the localized levels, similar to the graphene case. In GNRs, however, the relaxation effect is more significant near the edge sites, resulting in an additional energy gain. Thus, the formation energies tend to increase as the adsorption site changes from the edge to inner site. In the lowest energy configuration, the second H atom is located at the adjacent C site of the edge C–C dimer, in agreement with the other calculation [23].

If additional H atoms are adsorbed, they will be positioned along the ribbon edges until all the edge C atoms are passivated by hydrogen [23]. In this case, H adsorption may take place in two different ways on the edge C–C dimers. If the adsorption occurs on one side of the plane, the edge C–C dimers form a flat edge structure, without buckling relaxations (figure 6(a)). On the other hand, if the H atoms adsorb above and below the plane per unit cell, the edge dimers are tilted in the same direction, resulting in an α-type edge structure (figure 6(b)). In previous studies [20, 23, 40], two conformations with flat and α-type edge structures were considered for AGNRs, in which the edge atoms are fully passivated with two H atoms per edge C atom. As the orientation of edge dimers is affected by the type of adsorption, above or below the plane, there can be many edge structures, which are determined by the combination of α- and β-type edge dimers with opposite orientations, as shown in figures 6(c) and (d). An $\alpha\beta$-type edge structure consists of α- and β-type edge dimers, which are repeated after two unit cells,

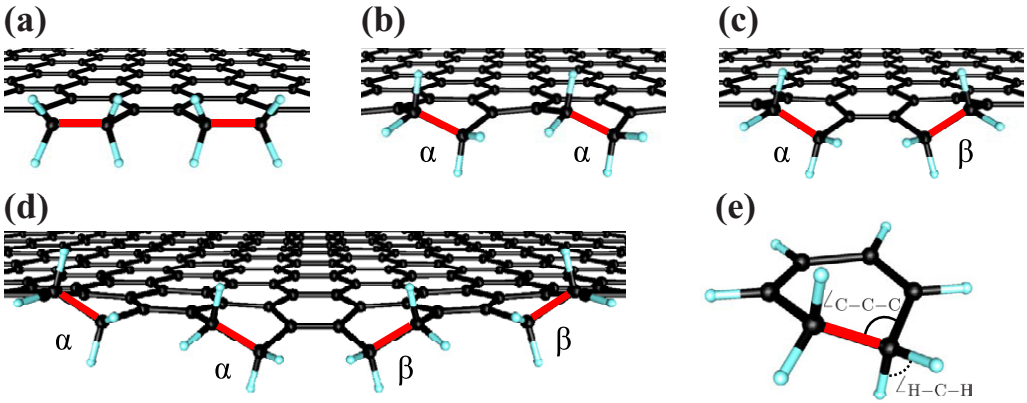

Figure 6. The atomic structures of four-edge conformations with (a) the flat, (b) α-type, (c) $\alpha\beta$-type and (d) $\alpha\alpha\beta\beta$-type edges in 29-AGNR, in which the edge atoms are fully passivated with two H atoms per edge C atom and (e) the local structure of 1,3-cyclohexadiene. Black and blue dots represent the C and H atoms, respectively, and red bars denote the C–C dimers.

Table 1. The formation energy differences (ΔE_f per edge C–C dimer) relative to the flat edge structure, the bond angles ($\angle_{C-C-C}$ and $\angle_{H-C-H}$) and the bond lengths (d_{C-C}) of the edge C–C dimers, and the energy gaps (E_{gap}) are listed for four different conformations of 29-AGNR with two H atoms per edge C atom, and compared with those of 1,3-cyclohexadiene.

Edge type	ΔE_f (eV)	$\angle_{C-C-C}$ (°)	$\angle_{H-C-H}$ (°)	d_{C-C} (Å)	E_{gap} (eV)
Flat	0	117.0	104.0	1.519	0.238
α-type	−0.060	111.8	106.3	1.511	0.233
$\alpha\beta$-type	−0.176	111.1	106.2	1.521	0.237
$\alpha\alpha\beta\beta$-type	−0.168	111.8	106.4	1.522	0.248
1,3-cyclohexadiene		111.4	106.0	1.532	

whereas the cell size becomes four times larger in an $\alpha\alpha\beta\beta$-type edge structure. We find that the α-type edge structure is more stable by 0.060 eV per edge dimer than the flat edge structure (table 1). In the $\alpha\beta$- and $\alpha\alpha\beta\beta$-type edge structures, their energies are further lowered to −0.176 and −0.168 eV per edge dimer, respectively.

For four-edge conformations considered here, the bond angles and bond lengths of the edge C–C dimers are listed and compared with those for 1,3-cyclohexadiene in table 1. It is interesting to note that the local geometry of a tilted armchair edge dimer is similar to that of 1,3-cyclohexadiene (Figure 6(e)). In 1,3-cyclohexadiene, the dimer bond length is 1.532 Å and the C–C–C and H–C–H bond angles are 111.4° and 106.0°, respectively, in good agreement with other calculations [41]. In the α-, $\alpha\beta$- and $\alpha\alpha\beta\beta$-type edge structures, which have tilted edge dimers, the bond angles are very similar to those of 1,3-cyclohexadiene. In the flat edge structure, as the edge dimers lie in the ribbon plane, the H–C–H bond angle decreases, whereas the C–C–C bond angle increases. The bond lengths of the edge C–C dimers are calculated to be

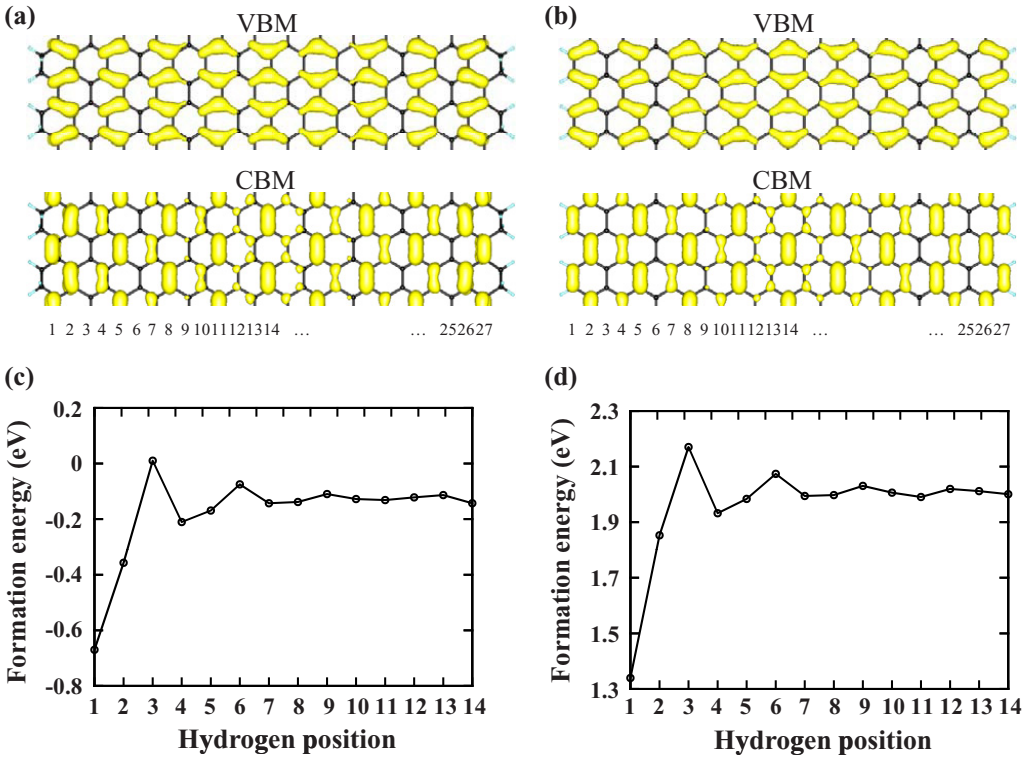

Figure 7. The charge distributions of the VBM and CBM states in (a) 29-AGNR with the $\alpha\beta$-type edge structure and (b) 27-AGNR with the edge atoms passivated with a single H atom per edge C atom. In (c) and (d), the formation energies of an additional H adsorbate in different dimer lines are compared for the supercells with two unit cells in (a) and (b), respectively. The C–C dimer lines are indexed by numbers in the reactive regions with the same effective ribbon width.

1.519, 1.511, 1.521 and 1.522 Å for the flat, α-, $\alpha\beta$- and $\alpha\alpha\beta\beta$-type edge structures, respectively, which are slightly smaller than that of 1,3-cyclohexadiene. In the α-type edge structure, the edge dimers experience more compressive strain, resulting in shorter bond length and thereby increasing the energy, compared with the $\alpha\beta$- and $\alpha\alpha\beta\beta$-type edge structures. As the energies of the $\alpha\beta$- and $\alpha\alpha\beta\beta$-type edge structures are similar, it is expected that other conformations with tilted edge dimers can be formed. We test an edge structure of $\alpha\alpha\alpha\beta\beta\beta$ type and find that it is unstable by about 0.02 eV against the $\alpha\beta$-type edge conformation, while it is still lower in energy than the flat and α-type edge structures.

The energy gaps are insensitive to the edge conformation, as shown in table 1. As the edge atoms are fully passivated by hydrogen, the energy gap is actually determined by the effective ribbon width, which corresponds to the unpassivated region and leads to the quantum confinement effect. If both of the edges of 29-AGNR are fully passivated by hydrogen, the effective width will be reduced by two dimer lines, being equal to that of 27-AGNR with a single H atom per edge C atom (figure 7). In fact, the energy gap of 27-AGNR with one H atom per edge C atom is calculated to be 0.237 eV, very close to those for four-edge conformations of 29-AGNR with the edge atoms fully passivated by hydrogen (table 1). For these 27- and

29-AGNRs, we find similar distributions of the charge densities for the VBM and CBM states (figures 7(a) and (b)), indicating that the effective ribbon widths are the same. Moreover, for an extra H atom adsorbed at the C sites in different dimer rows, the two AGNRs show similar formation energies, despite a small difference of about 0.1 eV in the first dimer line, which is caused by different relaxation effects. Thus, it is concluded that the effective ribbon width is a major factor in determining the band gap, consistent with other calculations [22, 23].

We find that there exists some similarity between our edge structures of GNRs and warping of graphene sheet. It is known that graphene edges are under compressive stress [42]–[45], which arises from the mismatch between the lattice constants in the edge and inner regions. As graphene edges are easily stretched along the axis, buckling or warping movement out of the plane, which lowers the energy, can take place. It was suggested that compressive stress is originated from repulsive interactions between the dangling bonds of the edge C atoms [44]. In AGNRs with a single H atom per edge C atom, the flat edge structure was suggested to be more favourable due to the stress release than warped edge conformations [42, 44, 45]. However, if each edge C atom is passivated by two H atoms, warping can occur even in the absence of compressive stress, as shown in figure 6. The physical origin of warping, in our case, is neither the repulsion between the dangling bonds nor the compressive stress, but the tendency for forming the sp^3-bonded network along the edges. The tilted edge dimers play a role in forming the warped structure. On the other hand, in zigzag GNRs, warping deformation is not likely to occur because edge C–C dimers do not exist at the zigzag edges; thus the flat edge structure becomes energetically more favorable.

In graphene, in which all of the C atoms are passivated by hydrogen, two hydrocarbon configurations were suggested to be favorable: a chair-like conformation with the H atoms alternating in the A and B sublattices on both sides of the plane and a boat-like conformation with the H atoms alternating in pairs [14]. The chair-like conformation was shown to be more favorable, with the energy difference of 55 meV per C atom. However, the energetics of these hydrocarbons are affected by the ribbon width and the edge structure in GNRs. In 29-AGNR with a single H atom per edge C atom, we assume that hydrogenation starts from the edge C atoms in a line-by-line manner, keeping the same configurations at both the edges (figures 8(a) and (b)). This assumption is reasonable because the H atoms prefer to adsorb at the outermost C atoms at the initial stage of hydrogenation. The formation energies per length along the edge are calculated and compared for the chair- and boat-like conformations in figure 8(c). For low coverages of H adsorbates, the edge structure plays an important role in forming the hydrocarbon conformation. Because the $\alpha\beta$-type edge structure is lower in energy than the α-type edge structure, the formation of the boat-like conformation is energetically more favorable when hydrogenation is continued up to the second C–C dimer line. As the H coverage increases, the chair-like conformation, which is derived from the α-type edge structure, is stabilized, similar to the stable hydrocarbon configuration of graphene. In the boat- and chair-like conformations, we find no significant difference in the band structure because the electronic structure mostly depends on the effective width of nanoribbons.

Finally, we investigate the transport properties of disordered GNRs with low coverages of additional H adsorbates ($n_H = 0.1$, 0.5 and 1%), in which adsorbates are random in both the A and B sublattices. In disordered 29-AGNR with a single H atom per edge C atom and the ribbon length (L) of 50 nm, additional H atoms are placed on only one side of the plane, without considering the relaxation effect at the edges, because the TB model is used. In addition, although it is energetically more favorable for hydrogenation to start from the edge sites to the

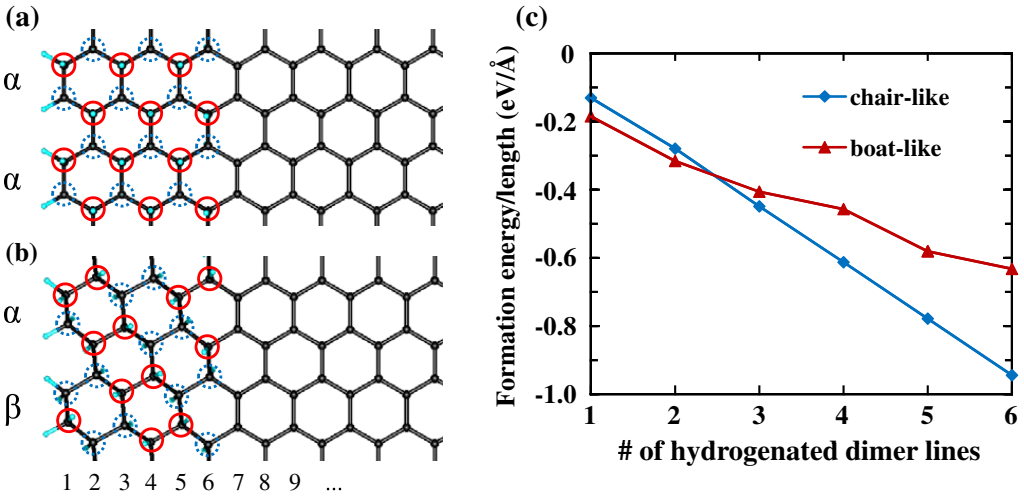

Figure 8. (a) The chair- and (b) boat-like conformations can be formed by hydrogenation in 29-AGNRs with the α- and $\alpha\beta$-type edge structures, respectively. Red and blue circles denote the H atoms adsorbed above and below the plane, respectively. (c) The formation energies per length along the edge are compared for different coverages of additional H adsorbates.

inner sites in a line-by-line manner (figure 8), it is more likely that the H atoms are randomly adsorbed in a realistic situation, especially at low coverages. Similar to disordered graphene by hydrogenation, the LIPRs are found to be greatly enhanced for the localized states near the neutrality point, and the energy range of localization grows with increasing n_{H} (figure 9(a)). Note that the localized levels even exist outside the intrinsic gap region, as shown in the averaged density of states (figure 9(b)), resulting in the larger mobility gap. When adsorbates are selectively diluted in the same sublattice, the gap regions are clearly found in the LIPR, with sharp peaks superimposed at the neutrality point, and the energy gap increases from 0.1 to 0.43 eV as n_{H} increases to 1%.

In the case of random H adsorbates, the logarithmic two-terminal conductances are plotted as a function of energy for specific samples with different H concentrations in figure 9(c). At the very low concentration of 0.1%, the conductances are severely suppressed in the energy window between -0.05 and 0.05 eV, which corresponds to the intrinsic energy gap of 29-AGNR. As n_{H} increases, the conductances fluctuate near the gap region and decrease further due to scattering between the localized states, in agreement with the LIPR results. To see the effect of sample size on conductance, we calculate the intrinsic conductance g in the scaling theory of localization [46], which is defined as $1/g = 1/g_{\mathrm{L}} - 1/2N_{\mathrm{c}}$, where N_{c} is the number of channels at the energy E and $1/2N_{\mathrm{c}}$ is the contact resistance. At each H concentration for a given ribbon length, we use 500–2000 configurations for the distribution of random adsorbates to calculate the ensemble average of $\ln g$, which is denoted by $\langle \ln g \rangle$. Figure 9(d) shows the variation of $\langle \ln g \rangle$ with the ribbon length at the energy $E = -0.3$ eV. It is clear that the conductance decays exponentially with respect to L, and the slope becomes larger as n_{H} increases, indicating the localization of the energy states. From the slopes, the localization lengths are estimated to be 47.6, 9.2 and 3.7 nm for $n_{\mathrm{H}} = 0.1$, 0.5 and 1%, respectively. At the very low concentration of $n_{\mathrm{H}} = 0.1\%$, although the localization length is very large, our results indicate that the localization still occurs for the band edge states.

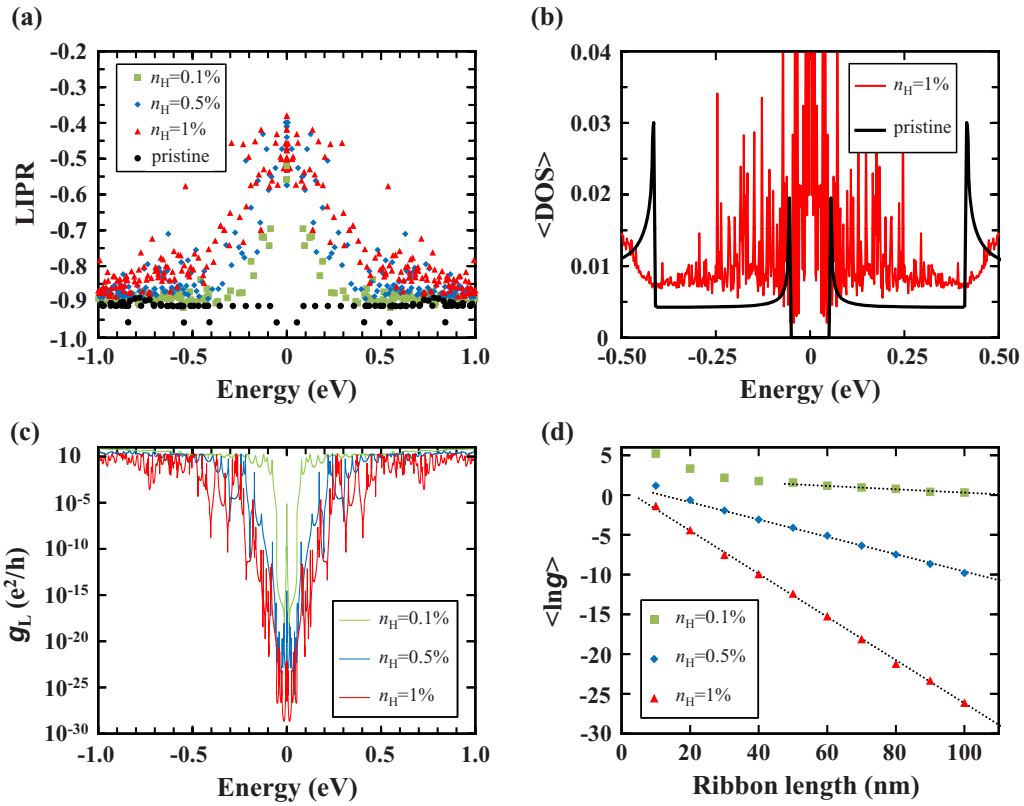

Figure 9. For disordered 29-AGNRs by hydrogenation, with the ribbon length of 50 nm, (a) the LIPR, (b) the averaged density of states ($\langle$DOS$\rangle$) and (c) the two-terminal conductance are plotted for low energies near the neutrality point. In (d), the averaged logarithmic conductances with $E = -0.3$ eV are plotted as a function of ribbon length. Black dots and lines represent the results of pristine 29-AGNR. The brackets in (b) and (d) denote the ensemble average over random configurations, whereas specific samples with different H concentrations are chosen in (a) and (c).

4. Summary

We have performed a numerical study of the electronic structure and transport properties of hydrogenated graphene and GNRs, based on the first-principles and TB calculations. In graphene, a selective dilution of H adsorbates in the same sublattice induces the band gap opening. As the defect levels are decoupled, the density of states exhibit sharp peaks superimposed near the neutrality point. From the analysis of the inverse participation ratio, we find that the localization of the band edge states becomes significant as the adsorbate density increases. If H adsorbates are random in both the A and B sublattices, the degenerate defect levels split due to the level repulsion, without creating the energy gap. The degree of localization by disorder is higher for the low-energy states near the neutrality point, and the localization extends to high-energy states with increasing the adsorbate density. In armchair-shaped GNRs, the effect of hydrogenation on the electronic structure is similar to that of graphene, except for the fact that GNRs have intrinsic energy gaps. Due to the structural relaxations of the edge

atoms, the edge sites are more reactive to hydrogen than the inner sites of the ribbon. When the edge atoms are fully passivated by hydrogen, the edge conformation is determined by the buckling of the edge C–C dimers. In disordered GNRs by hydrogenation, we also find that the energy states near the neutrality point are localized, exhibiting the decaying behavior of conductances with the sample size, similar to disordered graphene.

Acknowledgment

This work was supported by the National Research Foundation of Korea under grant no. NRF-2009-0093845.

References

[1] Castro Neto A H, Guinea F, Peres N M R, Novoselov K S and Geim A K 2009 *Rev. Mod. Phys.* **81** 109
[2] Novoselov K S, Geim A K, Morozov S V, Jiang D, Katsnelson M I, Grigorieva I V, Dubonos S V and Firsov A A 2005 *Nature* **438** 197
[3] Zhang Y, Tan Y-W, Stormer H L and Kim P 2005 *Nature* **438** 201
[4] Katsnelson M I, Novoselov K S and Geim A K 2006 *Nat. Phys.* **2** 620
[5] Morozov S V, Novoselov K S, Katsnelson M I, Schedin F, Elias D C, Jaszczak J A and Geim A K 2008 *Phys. Rev. Lett.* **100** 016602
[6] Son Y-W, Cohen M L and Louie S G 2006 *Phys. Rev. Lett.* **97** 216803
[7] Li X, Wang X, Zhang L, Lee S and Dai H 2008 *Science* **319** 1229
[8] Jiao L, Wang X, Diankov G, Wang H and Dai H 2010 *Nat. Nanotechnol.* **5** 321
[9] Vanević M, Stojanović V M and Kindermann M 2009 *Phys. Rev.* B **80** 045410
[10] Fürst J A, Pedersen J G, Flindt C, Mortensen N A, Brandbyge M, Pedersen T G and Jauho A-P 2009 *New J. Phys.* **11** 095020
[11] Eroms J and Weiss D 2009 *New J. Phys.* **11** 095021
[12] Balog R *et al* 2010 *Nature Mater.* **9** 315
[13] Wehling T O, Katsnelson M I and Lichtenstein A I 2009 *Phys. Rev.* B **80** 085428
[14] Sofo J O, Chaudhari A S and Barber G D 2007 *Phys. Rev.* B **75** 153401
[15] Elias D C *et al* 2009 *Science* **323** 610
[16] Bostwick A, McChesney J L, Emtsev K V, Seyller T, Horn K, Kevan S D and Rotenberg E 2009 *Phys. Rev. Lett.* **103** 056404
[17] Bang J and Chang K J 2010 *Phys. Rev.* B **81** 193412
[18] Boukhvalov D W, Katsnelson M I and Lichtenstein A I 2008 *Phys. Rev.* B **77** 035427
[19] Boukhvalov D W and Katsnelson M I 2008 *Nano Lett.* **8** 4373
[20] Wassmann T, Seitsonen A P, Marco Saitta A, Lazzeri M and Mauri F 2008 *Phys. Rev. Lett.* **101** 096402
[21] Wassmann T, Seitsonen A P, Marco Saitta A, Lazzeri M and Mauri F 2010 *J. Am. Chem. Soc.* **132** 3440
[22] Singh A K and Yakobson B I 2009 *Nano Lett.* **9** 1540
[23] Xiang H, Kan E, Wei S-H, Whangbo M-H and Yang J 2009 *Nano Lett.* **9** 4025
[24] Perdew J P, Burke K and Ernzerhof M 1996 *Phys. Rev. Lett.* **77** 3865
[25] Vanderbilt D 1990 *Phys. Rev.* B **41** R7892
[26] Kresse G and Furthmüller J 1996 *Comput. Mater. Sci.* **6** 15
[27] Monkhorst H J and Pack J D 1976 *Phys. Rev.* B **13** 5188
[28] Datta S 1995 *Electronic Transport in Mesoscopic Systems* (Cambridge: Cambridge University Press)
[29] Chan K T, Neaton J B and Cohen M L 2008 *Phys. Rev.* B **77** 235430
[30] Casolo S, Løvvik O M, Martinazzo R and Tantardini G F 2009 *J. Chem. Phys.* **130** 054704
[31] Duplock E J, Scheffler M and Lindan P J D 2004 *Phys. Rev. Lett.* **92** 225502

[32] Kang J, Bang J, Ryu B and Chang K J 2008 *Phys. Rev.* B **77** 115453
[33] Pereira V M, Guinea F, Lopes Dos Santos J M B, Peres N M R and Castro Neto A H 2006 *Phys. Rev. Lett.* **96** 036801
[34] Pereira V M, Lopes Dos Santos J M B and Castro Neto A H 2008 *Phys. Rev.* B **77** 115109
[35] Hornekær L, Šljivančanin Ž, Xu W, Otero R, Rauls E, Stensgaard I, Lægsgaard E, Hammer B and Besenbacher F 2006 *Phys. Rev. Lett.* **96** 156104
[36] Hornekær L, Rauls E, Xu W, Šljivančanin Ž, Otero R, Stensgaard I, Lægsgaard E, Hammer B and Besenbacher F 2006 *Phys. Rev. Lett.* **97** 186102
[37] Abrahams E, Anderson P W, Licciardello D C and Ramakrishnan T V 1979 *Phys. Rev. Lett.* **42** 673
[38] Lee P A and Ramakrishnan T V 1985 *Rev. Mod. Phys.* **57** 287
[39] Naumis G G 2007 *Phys. Rev.* B **76** 153403
[40] Lu Y H, Wu R Q, Shen L, Yang M, Sha Z D, Cai Y Q, He P M and Feng Y P 2009 *Appl. Phys. Lett.* **94** 122111
[41] Pye C C, Poirier R A, Jean Burnell D and Klapstein D 2009 *J. Mol. Struct. (Theochem)* **909** 66
[42] Jun S 2008 *Phys. Rev.* B **78** 073405
[43] Shenoy V B, Reddy C D, Ramasubramaniam A and Zhang Y W 2008 *Phys. Rev. Lett.* **101** 245501
[44] Huang B, Liu M, Su N, Wu J, Duan W, Gu B-L and Liu F 2009 *Phys. Rev. Lett.* **102** 166404
[45] Gan C K and Srolovitz D J 2009 arXiv:0909.4373
[46] Braun D, Hofstetter E, MacKinnon A and Montambaux G 1997 *Phys. Rev.* B **55** 7557